Geophysical Research Letters

RESEARCH LETTER
10.1029/2024GL112413

Monsoon-Frontal Interactions Drive Cyclone Biparjoy's Wake Recovery in the Arabian Sea

Siddhant Kerhalkar[1], Ankitha Kannad[2], Alex Kinsella[3], Amit Tandon[1,4], Janet Sprintall[2], and Craig M. Lee[5]

[1]School for Marine Science and Technology, University of Massachusetts Dartmouth, New Bedford, MA, USA, [2]Scripps Institution of Oceanography, University of California San Diego, La Jolla, CA, USA, [3]Department of Physical Oceanography, Woods Hole Oceanographic Institution, Woods Hole, MA, USA, [4]Mechanical Engineering Department, University of Massachusetts Dartmouth, North Dartmouth, MA, USA, [5]Applied Physics Laboratory, University of Washington, Seattle, WA, USA

Abstract Cyclone-generated cold wakes enhance productivity and impact local air-sea interaction, paths and intensities of subsequent storms in the region. However, in-situ observations of recovery across such wakes are rare. A cold wake in the Arabian Sea was surveyed using multiple shipboard instruments approximately 10 days after the passage of Cyclone Biparjoy in 2023. The wake, nearly 30 km wide, had a stronger (weaker) buoyancy gradient at its eastern (western) edge and assumed a downfront (upfront) orientation relative to the southwesterly monsoon winds. This resulted in notable asymmetry in the vertical structure of temperature, salinity and velocity at the edges of the wake, indicating the importance of Ekman Buoyancy Fluxes and Mixed Layer Eddies. While the wake recovery following a cyclone is often attributed to one-dimensional diurnal heating and cooling, these observations underscore the role of interactions between monsoon winds and underlying three-dimensional submesoscale processes for a slow-moving cyclone wake recovery.

Plain Language Summary Tropical cyclones are known to create a cold trail of water mixed upward from deeper waters, but observations of recovery of the wake back to pre-cyclone conditions are rare. These wakes play a crucial role in modulating availability of nutrients in the ocean, impact local atmosphere-ocean interaction and future passage of storms in the region. This study describes the structure of the wake after slow-moving Cyclone Biparjoy traverses the Arabian Sea in 2023 and highlights processes associated with the wake recovery. Our observations reveal that the wake is asymmetrical in its density and velocity structure. This is a result of the interaction between southwest monsoon winds and the density differences at the edges of the wake. Alongside the daily cycle of heating and cooling, these interactions foster small-scale three-dimensional processes, that are found to be crucial for the cold wake recovery back toward typical pre-cyclone conditions.

Key Points:

- Slow moving cyclone Biparjoy in the Arabian Sea triggers the formation of a cold, salty and productive wake, causing a 4°C drop in SSTs
- In-situ observations reveal the asymmetric recovery of the cold wake, with differences in mixed layer depth and buoyancy gradients at edges
- Winds interacting with the wake leads to Ekman Buoyancy Fluxes at sub-mesoscale length scales, emphasizing their role in wake's recovery

Supporting Information:

Supporting Information may be found in the online version of this article.

Correspondence to:

A. Tandon,
atandon@umassd.edu

Citation:

Kerhalkar, S., Kannad, A., Kinsella, A., Tandon, A., Sprintall, J., & Lee, C. M. (2025). Monsoon-frontal interactions drive cyclone biparjoy's wake recovery in the Arabian Sea. *Geophysical Research Letters*, *52*, e2024GL112413. https://doi.org/10.1029/2024GL112413

Received 9 SEP 2024
Accepted 30 JAN 2025

Author Contributions:

Conceptualization: Siddhant Kerhalkar, Amit Tandon, Janet Sprintall, Craig M. Lee
Data curation: Siddhant Kerhalkar, Ankitha Kannad, Janet Sprintall
Formal analysis: Siddhant Kerhalkar, Ankitha Kannad, Alex Kinsella
Funding acquisition: Alex Kinsella, Amit Tandon, Janet Sprintall, Craig M. Lee
Investigation: Siddhant Kerhalkar, Ankitha Kannad, Alex Kinsella, Amit Tandon, Janet Sprintall, Craig M. Lee
Project administration: Siddhant Kerhalkar, Amit Tandon, Janet Sprintall, Craig M. Lee

1. Introduction

Tropical cyclones, known for their high wind speeds, create a cold (and sometimes salty) wake due to increased upwelling and vertical mixing, causing sea surface temperatures (SSTs) within the wake to drop by 2°C–4°C (Stramma et al., 1986). However, this wake forms asymmetrically relative to the cyclone track, usually to the right of the cyclone eye in the Northern Hemisphere, due to wind stress anomalies generated by cyclone passage (Cornillon et al., 1987; Price, 1981; Sanabia & Jayne, 2020). While the cold wake's formation as a result of upwelling and enhanced turbulent mixing is well understood (D'Asaro, 2003; D'Asaro et al., 2007; Emanuel, 2003; Vincent et al., 2012; Yablonsky & Ginis, 2009), its recovery back to pre-cyclone conditions has received less attention. Understanding the evolution of the cold wake and its recovery is critical as it can significantly impact ocean heat transport, and the predictability of the path and intensity of subsequent storm systems that traverse the region (Emanuel, 2001; Gutiérrez Brizuela et al., 2023; Karnauskas et al., 2021; Pasquero & Emanuel, 2008). Significantly, cyclonic disturbances are often considered as the signature of the onset of Asian Monsoons, and hence, the cyclone wake conditions can impact the subsequent sub-seasonal predictions of monsoons (Evan & Camargo, 2011; Krishnamurti et al., 1981, 2007).

Early hypotheses suggested atmospheric surface forcing causes a wake recovery over 10 days or more (based on SST criterion defined in Price et al., 2008), but subsequent observational studies demonstrated that background advection also played a major role in the recovery of the cold wake (Johnston et al., 2020; Mrvaljevic et al., 2013). Numerical modeling results indicate that baroclinic instabilities at the edges of the cold wake lead to the formation

Supervision: Amit Tandon, Janet Sprintall, Craig M. Lee
Visualization: Siddhant Kerhalkar, Ankitha Kannad, Alex Kinsella
Writing – original draft: Siddhant Kerhalkar
Writing – review & editing: Siddhant Kerhalkar, Ankitha Kannad, Alex Kinsella, Amit Tandon, Janet Sprintall, Craig M. Lee

of submesoscale mixed-layer eddies (Fox-Kemper et al., 2008; Smith et al., 2019; Yi et al., 2024). These small-scale eddies cause the initially vertical isopycnals at fronts to slump and become nearly horizontal, creating a more stable state and thus contributing to the wake's recovery adiabatically (Figure S1d–S1f in Supporting Information S1, Haney et al., 2012; Mei & Pasquero, 2012). In addition, winds blowing parallel to the fronts at the wake's edges can create asymmetric recovery patterns through Ekman Buoyancy Fluxes (EBFs). Specifically, winds that oppose the surface thermal wind shear (upfront winds) can drive cross-front density advection via Ekman flow, resulting in stable wind-driven buoyancy fluxes. The sheared Ekman flow displaces the front and causes initially vertical buoyancy gradients to become more horizontal (and thus restratifying in nature), facilitating wake recovery adiabatically (Figure S1a–S1c in Supporting Information S1). Conversely, winds blowing in the direction of the surface thermal wind shear (downfront winds) lead to unstable conditions, enhancing mixing and deepening the mixed layer (thereby destratifying in nature), while also supporting frontogenesis and causing these fronts to remain relatively stationary (Thomas & Lee, 2005). Ekman Buoyancy Fluxes also interact with the restratifying effects of mixed-layer eddies and surface forcing, thereby accelerating the closure of cold wakes and driving complex recovery dynamics (Haney et al., 2012; Mahadevan et al., 2010).

Nonetheless, in-situ observations of lateral submesoscale processes affecting the recovery of the cold wake are lacking. For example, autonomous profilers such as Argo are typically not fast enough to capture the spatio-temporal evolution of the wake, even in highly networked field campaigns (e.g., D'Asaro et al., 2007; Johnston et al., 2021). While this challenge could be addressed with ship-based sampling, heightened surface waves associated with tropical cyclones along with other logistical obstacles render ship usage unfeasible unless the sampling strategy is critically timed, typically a few days after cyclone passage.

In this study, we utilize rare ship-based, in-situ observations conducted in the Arabian Sea during the "Enhancing Knowledge of the Arabian Sea Marine Environment through Science and Advanced Training (EKAMSAT)" program, which sample the wake of slow-moving Cyclone Biparjoy in June 2023. Our goal is to document the horizontal and vertical variability in the cyclone wake and its vicinity. We first provide an overview of the instruments and satellite products used in this study (Section 2), before describing the cold wake recovery using our unique observations and demonstrating the presence of submesoscale processes in this wake recovery (Section 3). The summary of our findings and their broader implications are discussed in Section 4.

2. Data and Methods

A combination of measurements collected by a ship-mounted flow-through thermosalinograph (TSG) and an Underway CTD (uCTD) profiler was employed to investigate the temperature and salinity structures within the cold wake resulting from Tropical Cyclone Biparjoy in the Arabian Sea between 17 and 20 June 2023. The TSG provides measurements at 4 m depth based on R/V Revelle's seawater intake, while the uCTD collected profiles over the top 250 m with a vertical resolution of 4 m and a temporal resolution of 10 min (an approximate horizontal resolution of 1.7 km). Meteorological conditions were measured from sensors housed on the ship's bow mast. The velocity structure within the cold wake was measured using the Hydrographic Doppler Sonar System (HDSS, Pinkel, 2012) over the top 550 m at a vertical resolution of 4.5 m. The mixed layer depth (MLD) is inferred from the uCTD measurements based on a 0.125 kg/m^3 density difference from surface values (Monterey & Levitus, 1997), while the isothermal layer depth (ILD) is defined based on a 0.5°C temperature difference with respect to the surface values (Levitus, 1983). The barrier layer thickness (BLT) is the difference between the ILD and the MLD.

We also utilize various level-3 remote sensing products such as the 3-Day product from Advanced Microwave Scanning Radiometer-2 (AMSR-2, Wentz et al., 2014) and NOAA 0.25° Daily Optimum Interpolation Sea Surface Temperature (OISST, Reynolds et al., 2007), a level-3 blended product combining microwave and infrared data, at a spatial resolution of nearly 25 km to examine the SSTs. Additionally, we assess the SST from level-2 versions of Moderate-resolution Imaging Spectroradiometer (MODIS) Aqua (NASA Goddard Space Flight Center, 2018) as well as Visible Infrared Imaging Radiometer Suite (VIIRS) on NOAA-20 and NPP platforms, with a spatial resolution of 750 m (Cao et al., 2013). We also use Advanced Very High Resolution Radiometer (AVHRR) SST data to obtain high-resolution nighttime images from the NOAA-18 and NOAA-19 platforms (Casey et al., 2010).

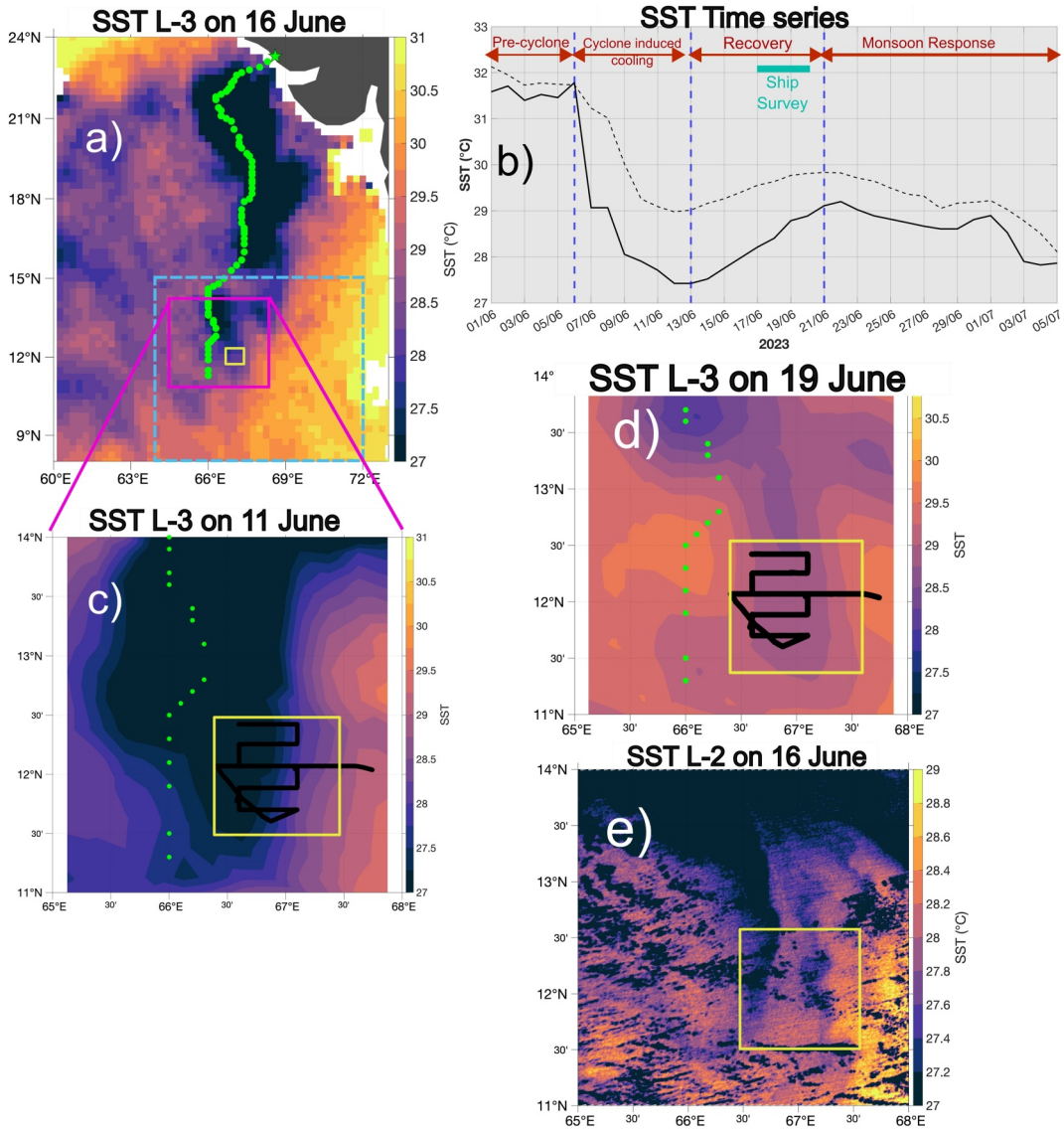

Figure 1. (a) SST from AMSR-2 on 16 June 2023. The green dots indicate the path of the cyclone Biparjoy (as obtained from IMD, 2023). (b) Time series of mean SSTs from AMSR-2 between 1 June and 5 July 2023. The ship surveyed the wake between 17-20 June and is indicated by cyan marker. Solid line indicates the mean SST over the smaller area around the ship operations in panel (a) (yellow solid box) while the dashed line indicates the same over the larger area in panel (a) (dashed blue box). (c) SST from AMSR-2 over the solid magenta box on 11 June 2023. (d) same as panel (c) but for 19 June 2023. Ship tracks are indicated by black lines in panels (c)–(d). (e) MODIS Aqua L-2 product on 16 June 2023 over the same solid magenta box in (a). The dots in panel (e) are flagged as clouds or ice contamination. Yellow solid box in panels (c)–(e) indicate the area around the ship operations.

3. Results

3.1. Remote Sensing of the Cyclone Wake Recovery

Cyclone Biparjoy, a slow-moving cyclone with translation speeds of 1–2 ms^{-1} (Figure S2a in Supporting Information S1), formed over the southern Arabian Sea on 5 June 2023. It reached its peak intensity as a category-3 cyclone and moved northward before making landfall over Gujarat, India on 15 June (IMD, 2023). The cyclone's passage resulted in the formation of the cold wake predominantly to the right of the track (Figure 1a), with a 4°C drop in SST over 7 days (Figure 1b) at the ship's operational area (yellow box in Figure 1a).

The cyclone wake begins to recover on 13 June, which is identified by a rise in SST of 1.7°C over 8 days (Figure 1b). With wind speeds and peak shortwave radiation in the wake area around 8 ms^{-1} and 940 W/m^2 respectively (Figure S3 in Supporting Information S1), the theoretical recovery period for the wake, if driven only by surface forcing, is estimated to be 18–29 days (see Text S1 in Supporting Information S1, Price, 1981; Haney et al., 2012). However, the rise in SST (or the surface recovery of the wake) ceases after 8 days instead (13-21 June, Figure 1b), reaching a steady state, although it fails to return to pre-cyclone values (Figure 1b). A large region of the southeastern Arabian Sea (marked by dashed blue line in Figure 1a) exhibits a similar lack of recovery to pre-cyclone SST. The large-scale forcing by the Southwest Monsoon (active between June and November each year) over the Arabian Sea prevents the SST from recovering to pre-cyclone values (e.g., Weller et al., 2002). Additionally, the presence of small-scale lateral processes due to the cyclone wake, such as mixed layer eddies as well as EBFs, can contribute to the ambiguities in the recovery timescale (e.g., Haney et al., 2012).

A comparison of satellite maps of SST between 11 June and 19 June reveals a thinning and warming trend of the wake (Figures 1c and 1d, Figure S4c–S4f in Supporting Information S1). The western edge of the wake moves eastward under the influence of Ekman flow while the eastern edge remains nearly stationary (Figures 1c and 1d). This differential motion hints at the presence of EBFs around the wake. Additionally, the high resolution infrared L-2 images of SST highlights the complex structure of the wake, with a region of warm water surrounding two cold water zones, each around 27.4°C (Figure 1e, see Text S2 in Supporting Information S1 for more detailed description). The edges of the wake also reveal its meandering nature, a detail that is often missed by coarser-resolution satellite products (Figure 1e). Given the meandering nature of the wake, which suggests the presence of lateral processes, and the observed wake recovery rate from satellite SSTs exceeding theoretical estimates based on surface forcing, we next analyze in-situ subsurface measurements. These measurements help explore the wake's structure and further emphasize the role of lateral processes in explaining the discrepancy between observed and surface-forcing-based recovery rates.

3.2. In-Situ Survey of the Wake

An in-situ survey from the ship's TSG and the uCTD system were conducted 10 days after the cyclone's passage to examine the structure of the generated wake (Figure S3 and S5 in Supporting Information S1). The winds during this period were generally south-westerly (consistent with the direction of winds during the monsoon season, Figure S3a in Supporting Information S1). In the near-surface layer, the edges of the wake are characterized by colder waters (a difference of 0.72°C) compared to those in the vicinity of the wake (Figure 2a). However, the core of the wake is slightly warmer than its edges. The core is also saltier (a 0.45 g kg^{-1} difference) and denser (a 0.39 kg/m^3 difference) than the surrounding waters. Due to this complex structure, the formation of the wake leads to the development of density fronts at its edges (despite the slight density compensation, see detailed secondary discussion in Text S2 in Supporting Information S1). Subsequent observations during this survey also reveal the small-scale meridional variability of the wake, highlighting its meandering nature (Figures 2a and 2b). Additionally, the unique wake structure (with the warm wake core and cold edges) mentioned earlier is not observed during the repeat section (see Text S2 in Supporting Information S1 and discussed further in Section 3.2.2).

The three-dimensional view of the sections reveals significant differences in the mixed layer structure throughout the wake and its vicinity (Figures 2c and 2d). Given the south-westerly winds and their orientation with respect to the wake-associated fronts, the presence of EBFs and mixed layer eddies is anticipated. These can potentially influence the upper ocean structure within the wake and its vicinity by causing an asymmetric recovery (Haney et al., 2012). To explore the vertical structure further, we next focus on the zonal section between the S2-E and S2-W waypoints. This section is the longest and captures both the eastward and westward edges of the wake (other sections only capture the westward edge, Figure 2).

3.2.1. Section Between S2-E and S2-W

Sharp contrasts in velocity and salinity define the western and eastern edges of the cyclone wake, both of which are characterized by outcropping isopycnals of higher surface density (Figure 3). As mentioned earlier, the core of the wake is associated with warm and salty waters, while colder waters are found at the edges of the wake, which are surrounded by warmer and fresher waters. Within the wake itself, a mixed layer depth (MLD) of 32 m and a BLT of 12 m are observed (Figures 3a and 3b). The wake is associated with weak eastward and northward flow

10.1029/2024GL112413

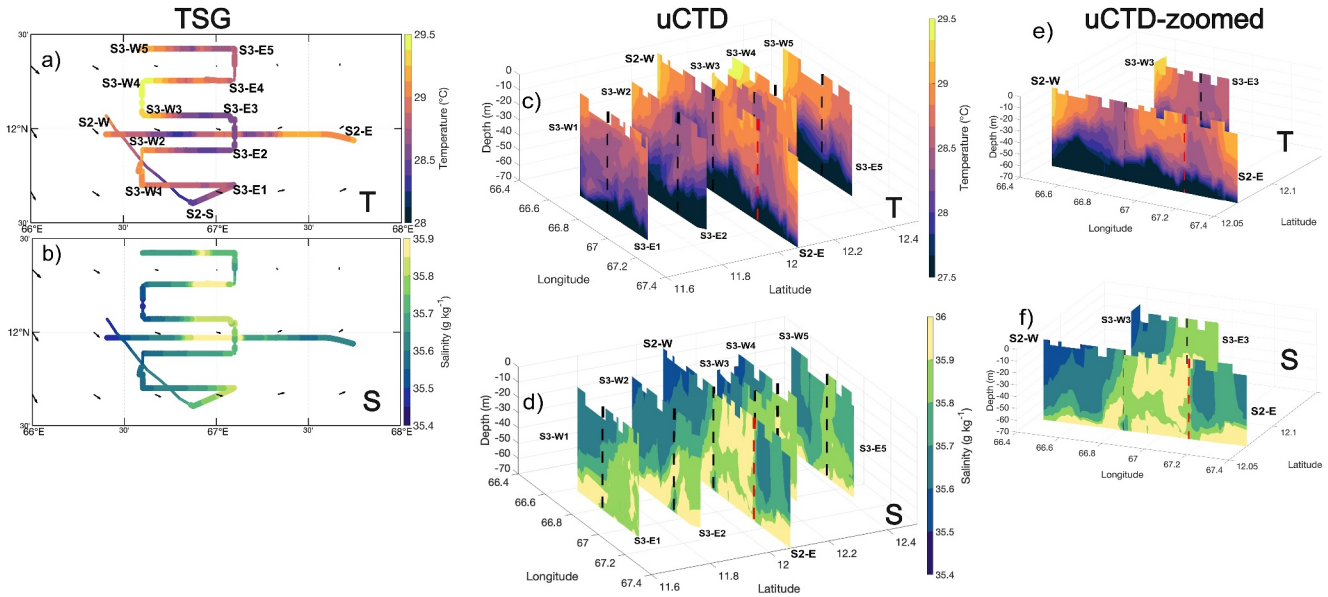

Figure 2. (a) Temperature and (b) salinity from the ship's TSG during the wake survey. (c) Temperature and (d) salinity from the uCTD during the wake survey. (e) and (f) are the same as (c) and (d) zooming into section S2-E to S2-W and section S3-E3 to S3-W3, respectively. The arrows in panels (a) and (b) are ocean surface currents from OSCAR (Dohan, 2021). Black dashed lines in panels (c)–(f) indicate the shift in meridional velocity over the mixed layer, marking the westward edge of the wake (see Figure 3 for more details). The red dashed line in panels (c)–(f) during the section S2-W to S2-E indicates the eastward edge of the wake. Panels (a), (c), (d), (e) and (f) feature various survey waypoints described in Table S2 in Supporting Information S1. NOTE: The section S3-E3 to S3-W3 is on the same latitude as section S2-E to S2-W. For ease of visualization, the section S3-E3 to S3-W3 has been offset northward by 0.1° in panels (c)–(f) while the section S2-W to S2-E has been offset southward by 0.1° in panels (a) and (b).

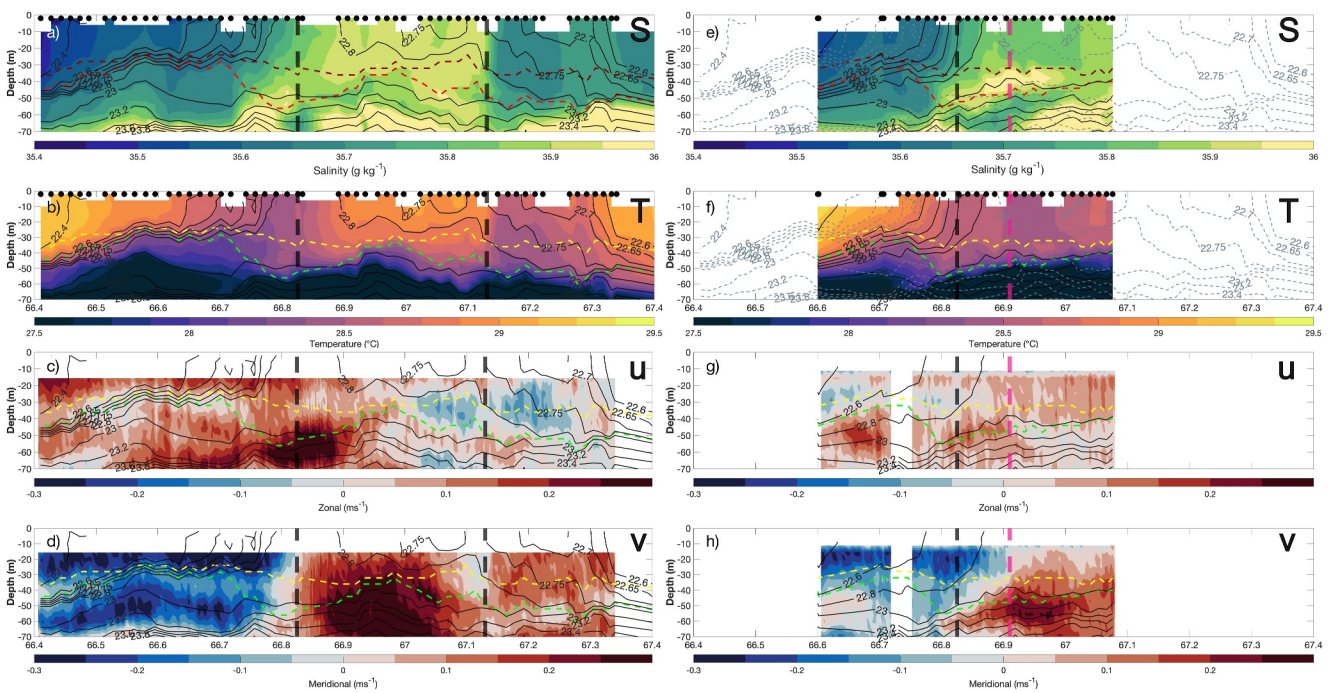

Figure 3. Vertical sections of (a) salinity, (b) temperature, (c) zonal velocity and (d) meridional velocity between S2-E and S2-W. The black dots in panels (a–b) are the individual uCTD profiles. Black contours in each panel indicate the isopycnals. The yellow (dark red in panel (a)) line in panels (b), (c), (d) indicate the MLD while the green (red in panel (a)) line indicate the ILD. Vertical black dashed lines indicate section dividers based on change in meridional velocity. Panels (e)–(h) are the same as panels (a)–(d) except the vertical section is between S3-W3 and S3-E3 (which is a shorter repeat section). The gray lines in panels (e) and (f) indicate the isopycnals from the original section (panels (a) and (b), respectively). The black dashed line in these panels is the westward edge of the wake in the original section (panels (a)–(d)) while the red dashed line is the westward edge of the wake in the S3-W3 and S3-E3 repeat section.

(Figures 3c and 3d). The velocities in the vicinity of the wake contrast sharply with those within the wake (as further discussed below, Figures 3c and 3d).

The S2-E to S2-W section reveals an asymmetric nature associated with the wake recovery. To the west of the wake, isopycnals slope downwards to the west. The MLD is slightly shallower (by about 4 m) compared to within the wake itself (Figures 3a and 3b). This region is characterized by weak eastward flow (around 0.1 ms^{-1}) and stronger southward velocities (0.3 ms^{-1}). This flow contrasts sharply to the flow within the wake, producing strong horizontal shear at the front (Figures 3c and 3d).

Isopycnals east of the wake are sloping down to the east, with steeper slopes than those observed on the western edge. This region is also characterized by smaller scale features of O (1 km) around 67.2° E (Figures 2a and 2b). The MLD in the eastern edge is deeper (by 9 m), while the BLT is thicker (by 8 m) when compared to within the wake. Compared to the western edge of the wake, the eastern edge has a deeper mixed layer (by about 12 m) and a BLT that is nearly twice as thick. The flow in the eastern edge of the wake is weakly westward and northward. Upon eliminating the effects of the background flow (by subtracting the mean velocities below the mixed layer depth along the whole section), evidence of weak convergence is observed in this area (Figure S6 in Supporting Information S1).

Understanding the buoyancy gradients in the wake is crucial as they serve as reservoirs of potential and kinetic energy, which can catalyze instabilities and impact upper-ocean mixing and stratification (Ferrari & Wunsch, 2009; Haine & Marshall, 1998). The buoyancy gradients change signs along section S2-E to S2-W since the denser (i.e., less buoyant) waters within the wake are surrounded by lighter (or more buoyant) waters (Figure 4a). Asymmetry is observed in the surface buoyancy gradients as well, where the peak magnitude of the buoyancy gradient at the eastern edge of the wake $\left(2.5 \times 10^{-7} s^{-2}\right)$ is 1.67 times higher than that on the western edge of the wake $\left(1.5 \times 10^{-7} s^{-2}\right)$ (Figure 4a). The buoyancy gradients associated with the cyclone wakes are of the same order of magnitude as within submesoscale meanders generated in the Gulf Stream (Shcherbina et al., 2015).

Estimates of buoyancy gradients (from uCTD) and south-westerly wind stresses (from ship-based meteorological measurements, Figure 4b) are used to calculate the Ekman buoyancy flux (EBF $= \frac{\tau_y}{\rho_o f} \frac{\partial b}{\partial x}$, where ρ_o is the reference density, f is the coriolis frequency, τ_y is the meridional wind stress while $\frac{\partial b}{\partial x}$ is the horizontal buoyancy gradient in the zonal direction). The temperature variation part of EBF is converted into equivalent Ekman heat fluxes (EHF $= \frac{\rho_o c_p (EBF_t)}{\alpha g}$, where $EBF_t = \frac{\tau_y}{\rho_o f} \alpha g \frac{\partial T}{\partial x}$. c_p is the specific heat of water, α is the thermal expansion coefficient and g is the acceleration due to the gravity). Ekman heat flux values are found to be of O (500 W/m^2) at both edges of the wake (Figure 4b), significantly exceeding the observed surface heat fluxes, which have a daily average of approximately 150 W/m^2 (Figure S3b in Supporting Information S1). Such elevated EHF values are capable of triggering submesoscale processes like frontal slumping and steepening (D'Asaro et al., 2011; Brannigan et al., 2015). This is further confirmed by calculating the Rossby number and Richardson number throughout the section, where these numbers are O(1) near the edges of the wake (Thomas et al., 2008).

With respect to the orientation of the winds (Figure 4b) and the density gradients (Figures 3a–3d and 4a), the western edge of the wake is forced by upfront wind component, while the eastern edge is influenced by a significant downfront wind component. This explains the asymmetry observed in the vertical structure of the wake, where the west side (forced by upfront winds) is undergoing restratification (and hence shallower MLDs), while the east side (forced by downfront winds) has a stronger buoyancy gradient as a result of destratification (Figure 4c). This is consistent with the sign of the EHFs, which are stabilizing at the western edge of the wake and are destabilizing at the eastern edge. Despite the destabilizing effect from the EBFs at the eastern edge of the wake, the isopycnals are not fully vertical but slope down to the east, indicating ongoing restratification. Previous studies have shown that a front can undergo restratification even with a destratifying downfront configuration in the presence of mixed layer eddies (e.g., Mahadevan et al., 2010). Thus, the restratification at the eastern edge, despite its downfront configuration, provides indirect evidence of the presence of mixed layer eddies. Inferences about active restratification arise from the fact that the fronts in this case are yet to fully geostrophically adjust (a front is considered fully geostrophically adjusted when $N^2 = \left(\frac{\partial b}{\partial x}\right)^2 / f^2$, where N^2 is the vertical stratification, Tandon & Garrett, 1994).

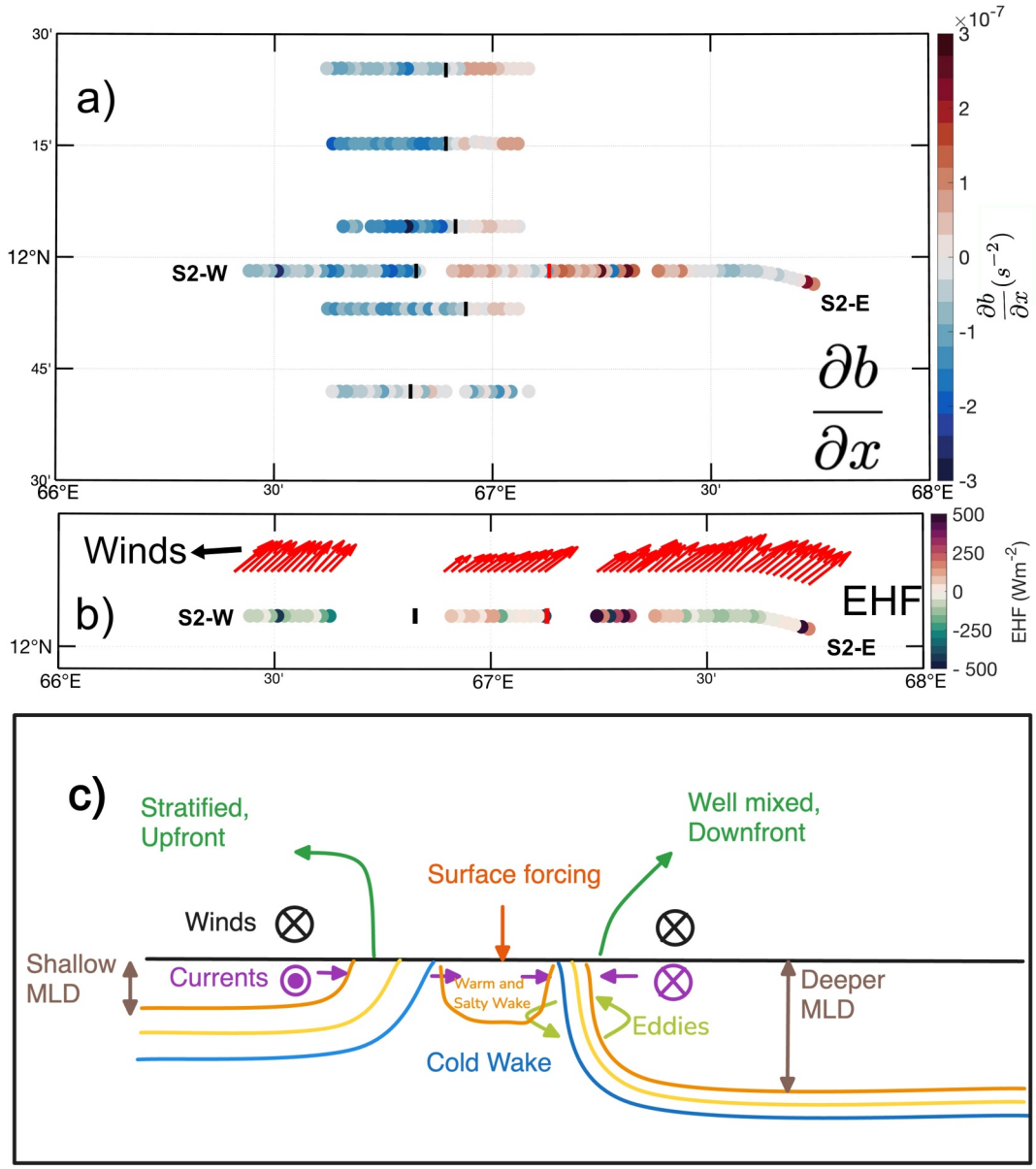

Figure 4. (a) Surface buoyancy gradients from the ship's survey in the wake and its vicinity. NOTE: The section S2-E to S2-W is offset by 0.1° to the south as to avoid overlap between repeating sections. (b) Ekman heat flux (EHF) in the section S2-W to S2-E. The red arrows indicate concurrent wind directions. Black line marker and Red line marker in panels (a)–(b) indicate the westward edge and eastward edge of the wake respectively. (c) Schematic explaining the forcing conditions and the asymmetric response of the cold wake in section S2-W to S2-E (adapted from Haney et al., 2012).

Using the theoretical scalings derived in Haney et al. (2012), we estimate that the separate recovery time scales associated with the surface forcing (T_{sf}), EBFs (T_{ebf}) and mixed layer eddies (T_{eddy}) are 29.6 ± 7, 25.4 ± 6 and 38.4 ± 8 days respectively (see Text S1 in Supporting Information S1 for details of the scaling analysis). Thus, while EBFs alone lead to a slightly faster recovery rate, the combination of surface forcing and EBFs yields an estimated recovery timescale of 9 ± 2 days, while the combination of all of the above processes (including mixed layer eddies) results in an estimated recovery timescale of 7 ± 1 day (Text S1 in Supporting Information S1). This timescale closely aligns with the observed SST recovery (Figure 1b), however high-resolution numerical simulations are needed to further validate the recovery timescales quoted here. Nonetheless, this scaling analysis highlights the role of lateral processes like EBFs and mixed layer eddies in causing a faster recovery of the wake, underscoring the important role of wind-front coupling in such cases. Given the enhanced shear at the base of the

mixed layer within the wake (Figures 3c and 3d), double-diffusive processes are not a significant contributor to the wake recovery (e.g., Kunze, 1990).

3.2.2. Section Between S3-E3 and S3-W3: Repeat Section

As mentioned previously, the zonal sections of the in-situ survey highlights slight meridional variations within the wake, thereby revealing the meandering nature of the wake (Figures 2 and 4a). The repeat section between S3-E3 and S3-W3 (referred to as the repeat section hereafter) was conducted along the same latitude as the section S2-E to S2-W (original section hereafter, Figure 2, Table S2 in Supporting Information S1) nearly 28 hours later, and hence provided an opportunity to understand the variability of the wake.

The repeat section is shorter and hence does not capture the eastward edge of the wake unlike the original section described in Section 3.2.1 (Figures 2 and 3e–3h). However, the vertical structure of the repeat section is similar to the original section described above. The main difference is that the westward edge of the wake is displaced by 10 km to the east (Figures 3e–3h) during the repeat section survey. This is also consistent with the disappearance of the unique wake structure (characterized by a warm core and cold edges) during the repeat section, as observed in both in-situ (Figures 2a and 2b) and satellite observations (Figure S7c in Supporting Information S1). This displacement could be due to several factors, including Ekman transport due to the south-westerly monsoon winds, advection by the background flow and/or near-inertial currents. While Ekman transport and advection are plausible causes, the near-inertial currents are less likely since Cyclone Biparjoy was initially a slow-moving cyclone (with translation speed of 1–2 ms^{-1}, Figure S2a in Supporting Information S1), resulting in a smaller near-inertial response (Figure S2c in Supporting Information S1, Price, 1981). Near-inertial currents calculated using the slab model (Pollard & Millard, 1970) forced by MERRA-2 reanalysis product (Global Modeling and Assimilation Office (GMAO), 2015) were roughly 0.05 ms^{-1}, which is about one-sixth of the observed currents in this section (Figures 3d and 3h).

4. Summary and Discussion

Cyclone Biparjoy created a cold wake over the Arabian Sea in June 2023. SST began recovering post-cyclone, reaching steady state in 8 days, far more rapidly than the 18–29 days predicted by one-dimensional models forced by winds and surface fluxes (Haney et al., 2012; Price et al., 2008). The scaling of recovery timescales from Haney et al. (2012) using the observed parameters reveals that the Ekman Buoyancy Flux (EBF), surface forcing and mixed layer eddies have similar recovery timescales when acting in isolation (25.4 ± 6, 29.6 ± 7 and 38.4 ± 8 days respectively). However, an estimated recovery timescale of 7 days due to the combination of these processes closely matches the recovery timescale observed from satellite SSTs, highlighting the role of submesoscale processes in speeding up the recovery of the wake (Figure 1b).

In-situ observations across the wake reveal its asymmetrical structure during the recovery as a result of the presence of EBF. The asymmetry is caused due to the imposition of southwesterly winds on the wake, which leads to upfront forcing on the wake's western edge, leading to shallower MLDs and hence restratifying. In contrast, the wake's eastern edge is forced by downfront winds, with deeper MLD and a presumably destratifying nature. However, observations of sloped isopycnals at the eastern edge of the wake indicate a weak stratification, providing indirect evidence of the presence of mixed layer eddies (Fox-Kemper et al., 2008; Mahadevan et al., 2010). The EBF (O (500 W/m^2)) as well as Rossby and Richardson numbers (both O(1)) associated with the cyclone wake were found to be sufficient to drive submesoscale processes at the edges of the wake as a result of the density gradients and their interaction with the winds. Given that Cyclone Biparjoy was a slow-moving storm, the near-inertial currents were small. Additionally, in-situ observations across the wake also reveal its unique structure characterized by a warmer and saltier core with colder edges, surrounded by warmer and fresher waters. Such small scale differences within the wake structure are challenging to observe with coarser satellite measurements.

These results present the first in-situ observations of a post-cyclone wake recovery in the Arabian Sea. Our observations emphasize the significance of the interaction between monsoon winds and the underlying three-dimensional submesoscale fronts in shaping the wake of a slow-moving cyclone through Ekman buoyancy fluxes. This contrasts with faster-moving cyclones, where near-inertial currents primarily dominate the wake evolution (Price, 1981). Understanding this recovery and the associated processes is vital, as it can influence

ocean heat transport, nutrient availability (Babin et al., 2004), coral health (Dobbelaere et al., 2024), and the predictability of future cyclones and sub-seasonal weather patterns.

Data Availability Statement

Data from the instruments are embargoed under agreement between the U.S. and India until 2029 as one step in fostering the international collaboration. This time frame is intended to allow for students and postdoctoral researchers supported under the project to have sufficient time to publish observation-based results. After the embargo period, data may be requested from the corresponding author. The satellite data for AMSR-2 as well as OISST were obtained from www.remss.com, while the level-2 products of MODIS-Aqua and VIIRS were obtained from https://oceancolor.gsfc.nasa.gov/cgi/browse.pl?sen=amod. AVHRR SST data were obtained from https://search.earthdata.nasa.gov/search while OSCAR currents were obtained from https://podaac.jpl.nasa.gov/dataset/OSCAR_L4_OC_INTERIM_V2.0. MERRA-2 data were obtained from https://disc.gsfc.nasa.gov/datasets/M2T1NXLND_5.12.4/summary.

Acknowledgments
The authors gratefully acknowledge the support of the US Office of Naval Research for the EKAMSAT-ASTraL Department Research Initiative. S. Kerhalkar and A. Tandon received support from N00014-23-1-2054, A. Kannad and J. Sprintall from N00014-23-1-2091, A. Kinsella from N00014-23-1-2471, and C. M. Lee from N00014-23-1-2085. A. Tandon also acknowledges support from N00014-23-1-2473. The authors extend their gratitude to the Captain, crew, and science party of R/V Roger Revelle during the EKAMSAT pilot field campaign for their invaluable assistance with data collection. S. K. acknowledges the support of the Associate Provost's office, University of Massachusetts Dartmouth, through the Distinguished Doctoral Fellowship. Special thanks to Joaquim Goes, Charles Kovach, and Sherwin Ladner for their assistance in obtaining L-2 satellite images. The authors also thank Elizabeth J. Thompson, Ludovic Bariteau, Byron Blomquist, Chris Fairall and Sergio Pezoa (from NOAA PSL as a part of NOAA Global Ocean Monitoring and Observations program) as well as Joe (Harindra) Fernando, Jay Orson Hyde and Griffin Modjeski (from University of Notre Dame as a part of EKAMSAT-ASTraL) for their role in QC'ing the surface meteorological measurements presented here. Thanks to Eric D'Asaro for insightful discussions. The authors would also like to thank the editor, Dr. Kris Karnauskas, and two anonymous reviewers for their constructive feedback that helped improve this manuscript. Lastly, this paper is dedicated to the memory of Sean Haney, who would have been happy to see these observations in line with his numerical results.

References

Babin, S., Carton, J., Dickey, T., & Wiggert, J. (2004). Satellite evidence of hurricane-induced phytoplankton blooms in an oceanic desert. *Journal of Geophysical Research*, *109*(C3). https://doi.org/10.1029/2003jc001938

Brannigan, L., Marshall, D. P., Naveira-Garabato, A., & Nurser, A. G. (2015). The seasonal cycle of submesoscale flows. *Ocean Modelling*, *92*, 69–84. https://doi.org/10.1016/j.ocemod.2015.05.002

Cao, C., De Luccia, F. J., Xiong, X., Wolfe, R., & Weng, F. (2013). Early on-orbit performance of the visible infrared imaging radiometer suite onboard the Suomi National Polar-Orbiting Partnership (S-NPP) satellite. *IEEE Transactions on Geoscience and Remote Sensing*, *52*(2), 1142–1156. https://doi.org/10.1109/tgrs.2013.2247768

Casey, K. S., Brandon, T. B., Cornillon, P., & Evans, R. (2010). The past, present, and future of the AVHRR Pathfinder SST program. *Oceanography from space*, 273–287. https://doi.org/10.1007/978-90-481-8681-5_16

Cornillon, P., Stramma, L., & Price, J. F. (1987). Satellite measurements of sea surface cooling during hurricane Gloria. *Nature*, *326*(6111), 373–375. https://doi.org/10.1038/326373a0

D'Asaro, E., Lee, C., Rainville, L., Harcourt, R., & Thomas, L. (2011). Enhanced turbulence and energy dissipation at ocean fronts. *Science*, *332*(6027), 318–322. https://doi.org/10.1126/science.1201515

D'Asaro, E. A. (2003). The ocean boundary layer below Hurricane Dennis. *Journal of Physical Oceanography*, *33*(3), 561–579. https://doi.org/10.1175/1520-0485(2003)033<0561:toblbh>2.0.co;2

D'Asaro, E. A., Sanford, B., Niiler, P. P., & Terrill, E. J. (2007). Cold wake of hurricane Frances. *Geophysical Research Letters*, *34*(15). https://doi.org/10.1029/2007gl030160

Dobbelaere, T., Dekens, A., Saint-Amand, A., Alaerts, L., Holstein, D. M., & Hanert, E. (2024). Hurricanes enhance coral connectivity but also superspread coral diseases. *Global Change Biology*, *30*(6), e17382. https://doi.org/10.1111/gcb.17382

Dohan, K. (2021). Ocean surface current analyses real-time (OSCAR) surface currents - near real time 0.25 degree (version 2.0). *NASA Physical Oceanography Distributed Active Archive Center*. https://doi.org/10.5067/OSCAR-25N20

Emanuel, K. (2001). Contribution of tropical cyclones to meridional heat transport by the oceans. *Journal of Geophysical Research*, *106*(D14), 14771–14781. https://doi.org/10.1029/2000jd900641

Emanuel, K. (2003). Tropical cyclones. *Annual Review of Earth and Planetary Sciences*, *31*(1), 75–104. https://doi.org/10.1146/annurev.earth.31.100901.141259

Evan, A. T., & Camargo, S. J. (2011). A climatology of Arabian Sea cyclonic storms. *Journal of Climate*, *24*(1), 140–158. https://doi.org/10.1175/2010jcli3611.1

Ferrari, R., & Wunsch, C. (2009). Ocean circulation kinetic energy: Reservoirs, sources, and sinks. *Annual Review of Fluid Mechanics*, *41*(1), 253–282. https://doi.org/10.1146/annurev.fluid.40.111406.102139

Fox-Kemper, B., Ferrari, R., & Hallberg, R. (2008). Parameterization of mixed layer eddies. Part I: Theory and diagnosis. *Journal of Physical Oceanography*, *38*(6), 1145–1165. https://doi.org/10.1175/2007jpo3792.1

Global Modeling and Assimilation Office (GMAO). (2015). MERRA-2 tavg1_2d_lnd_Nx: 2d,1-Hourly,Time-Averaged,Single-Level,Assimilation,Land surface diagnostics V5.12.4. Greenbelt, MD, USA. *Goddard Earth Sciences Data and Information Services Center (GES DISC)*. https://doi.org/10.5067/RKPHT8KC1Y1T

Gutiérrez Brizuela, N., Alford, M. H., Xie, S.-P., Sprintall, J., Voet, G., Warner, S. J., et al. (2023). Prolonged thermocline warming by near-inertial internal waves in the wakes of tropical cyclones. *Proceedings of the National Academy of Sciences*, *120*(26), e2301664120. https://doi.org/10.1073/pnas.2301664120

Haine, T. W., & Marshall, J. (1998). Gravitational, symmetric, and baroclinic instability of the ocean mixed layer. *Journal of Physical Oceanography*, *28*(4), 634–658. https://doi.org/10.1175/1520-0485(1998)028<0634:gsabio>2.0.co;2

Haney, S., Bachman, S., Cooper, B., Kupper, S., McCaffrey, K., Van Roekel, L., et al. (2012). Hurricane wake restratification rates of one-two-and three-dimensional processes. *Journal of Marine Research*, *70*(6), 824–850. Retrieved from https://elischolar.library.yale.edu/journal_of_marine_research/361

IMD. (2023). Extremely severe cyclonic storm "BIPARJOY" over the Arabian Sea (6th-19th June, 2023): A report. Retrieved from https://rsmcnewdelhi.imd.gov.in/download.php?path=uploads/report/26/26_49adec_ESCSReport_22June%202023%20(Approved).pdf

Johnston, T. S., Rudnick, D. L., Brizuela, N., & Moum, J. N. (2020). Advection by the North Equatorial Current of a cold wake due to multiple typhoons in the western Pacific: Measurements from a profiling float array. *Journal of Geophysical Research: Oceans*, *125*(4), e2019JC015534. https://doi.org/10.1029/2019jc015534

Johnston, T. S., Wang, S., Lee, C.-Y., Moum, J. N., Rudnick, D. L., & Sobel, A. (2021). Near-inertial wave propagation in the wake of super typhoon mangkhut: Measurements from a profiling float array. *Journal of Geophysical Research: Oceans*, *126*(2), e2020JC016749. https://doi.org/10.1029/2020jc016749

Karnauskas, K. B., Zhang, L., & Emanuel, K. A. (2021). The feedback of cold wakes on tropical cyclones. *Geophysical Research Letters*, *48*(7), e2020GL091676. https://doi.org/10.1029/2020gl091676

Krishnamurti, T., Ardanuy, P., Ramanathan, Y., & Pasch, R. (1981). On the onset vortex of the summer monsoon. *Monthly Weather Review*, *109*(2), 344–363. https://doi.org/10.1175/1520-0493(1981)109<0344:otovot>2.0.co;2

Krishnamurti, T., Chakraborty, A., Krishnamurti, R., Dewar, W. K., & Clayson, C. A. (2007). Passage of intraseasonal waves in the subsurface oceans. *Geophysical Research Letters*, *34*(14). https://doi.org/10.1029/2007gl030496

Kunze, E. (1990). The evolution of salt fingers in inertial wave shear. *Journal of Marine Research*, *48*(3), 471–504. Retrieved from https://elischolar.library.yale.edu/journal_of_marine_research/1977

Levitus, S. (1983). Climatological atlas of the world ocean. *Eos, Transactions American Geophysical Union*, *64*(49), 962–963. https://doi.org/10.1029/eo064i049p00962-02

Mahadevan, A., Tandon, A., & Ferrari, R. (2010). Rapid changes in mixed layer stratification driven by submesoscale instabilities and winds. *Journal of Geophysical Research*, *115*(C3). https://doi.org/10.1029/2008jc005203

Mei, W., & Pasquero, C. (2012). Restratification of the upper ocean after the passage of a tropical cyclone: A numerical study. *Journal of Physical Oceanography*, *42*(9), 1377–1401. https://doi.org/10.1175/jpo-d-11-0209.1

Monterey, G. I., & Levitus, S. (1997). Seasonal variability of mixed layer depth for the world ocean.

Mrvaljevic, R. K., Black, P. G., Centurioni, L. R., Chang, Y.-T., D'Asaro, E. A., Jayne, S. R., et al. (2013). Observations of the cold wake of Typhoon Fanapi (2010). *Geophysical Research Letters*, *40*(2), 316–321. https://doi.org/10.1029/2012gl054282

NASA Goddard Space Flight Center, O. B. P. G. (2018). Moderate-resolution imaging spectroradiometer (MODIS) Aqua ocean color data. *NASA OB.DAAC*. [dataset]. https://doi.org/10.5067/AQUA/MODIS/L2/OC/2018

Pasquero, C., & Emanuel, K. (2008). Tropical cyclones and transient upper-ocean warming. *Journal of Climate*, *21*(1), 149–162. https://doi.org/10.1175/2007jcli1550.1

Pinkel, R. (2012). Velocity imprecision in finite-beamwidth shipboard Doppler sonar: A first-generation correction algorithm. *Journal of Atmospheric and Oceanic Technology*, *29*(10), 1569–1580. https://doi.org/10.1175/jtech-d-12-00041.1

Pollard, R. T., & Millard, R. (1970). Comparison between observed and simulated wind-generated inertial oscillations. *Deep-Sea Research and Oceanographic Abstracts*, *17*(4), 813–821. https://doi.org/10.1016/0011-7471(70)90043-4

Price, J. F. (1981). Upper ocean response to a hurricane. *Journal of Physical Oceanography*, *11*(2), 153–175. https://doi.org/10.1175/1520-0485(1981)011<0153:uortah>2.0.co;2

Price, J. F., Morzel, J., & Niiler, P. P. (2008). Warming of SST in the cool wake of a moving hurricane. *Journal of Geophysical Research*, *113*(C7). https://doi.org/10.1029/2007jc004393

Reynolds, R. W., Smith, T. M., Liu, C., Chelton, D. B., Casey, K. S., & Schlax, M. G. (2007). Daily high-resolution-blended analyses for sea surface temperature. *Journal of Climate*, *20*(22), 5473–5496. https://doi.org/10.1175/2007jcli1824.1

Sanabia, E. R., & Jayne, S. R. (2020). Ocean observations under two major hurricanes: Evolution of the response across the storm wakes. *AGU Advances*, *1*(3), e2019AV000161. https://doi.org/10.1029/2019av000161

Shcherbina, A. Y., Sundermeyer, M. A., Kunze, E., D'Asaro, E., Badin, G., Birch, D., et al. (2015). The LatMix summer campaign: Submesoscale stirring in the upper ocean. *Bulletin of the American Meteorological Society*, *96*(8), 1257–1279. https://doi.org/10.1175/bams-d-14-00015.1

Smith, T. A., Jolliff, J. K., Walker, N. D., & Anderson, S. (2019). Biophysical submesoscale processes in the wake of hurricane ivan: Simulations and satellite observations. *Journal of Marine Science and Engineering*, *7*(11), 378. https://doi.org/10.3390/jmse7110378

Stramma, L., Cornillon, P., & Price, J. F. (1986). Satellite observations of sea surface cooling by hurricanes. *Journal of Geophysical Research*, *91*(C4), 5031–5035. https://doi.org/10.1029/jc091ic04p05031

Tandon, A., & Garrett, C. (1994). Mixed layer restratification due to a horizontal density gradient. *Journal of Physical Oceanography*, *24*(6), 1419–1424. https://doi.org/10.1175/1520-0485(1994)024<1419:mlrdta>2.0.co;2

Thomas, L. N., & Lee, C. M. (2005). Intensification of ocean fronts by down-front winds. *Journal of Physical Oceanography*, *35*(6), 1086–1102. https://doi.org/10.1175/jpo2737.1

Thomas, L. N., Tandon, A., & Mahadevan, A. (2008). Submesoscale processes and dynamics. *Ocean modeling in an Eddying Regime*, *177*, 17–38. https://doi.org/10.1029/177gm04

Vincent, E. M., Lengaigne, M., Madec, G., Vialard, J., Samson, G., Jourdain, N. C., et al. (2012). Processes setting the characteristics of sea surface cooling induced by tropical cyclones. *Journal of Geophysical Research*, *117*(C2). https://doi.org/10.1029/2011jc007396

Weller, R., Fischer, A., Rudnick, D., Eriksen, C., Dickey, T., Marra, J., et al. (2002). Moored observations of upper-ocean response to the monsoons in the Arabian Sea during 1994–1995. *Deep Sea Research Part II: Topical Studies in Oceanography*, *49*(12), 2195–2230. https://doi.org/10.1016/s0967-0645(02)00035-8

Wentz, F., Meissner, T., Gentemann, C., Hilburn, K., & Scott, J. (2014). Remote sensing systems GCOM-W1 AMSR2 3-day environmental suite on 0.25 deg grid, version 08.2 [dataset]. *Remote Sensing Systems, Santa Rosa, CA*. Retrieved from www.remss.com/missions/amsr

Yablonsky, R. M., & Ginis, I. (2009). Limitation of one-dimensional ocean models for coupled hurricane–ocean model forecasts. *Monthly Weather Review*, *137*(12), 4410–4419. https://doi.org/10.1175/2009mwr2863.1

Yi, Z., Qiu, C., Wang, D., Cai, Z., Yu, J., & Shi, J. (2024). Submesoscale kinetic energy induced by vertical buoyancy fluxes during the tropical cyclone Haitang. *Journal of Geophysical Research: Oceans*, *129*(7), e2023JC020494. https://doi.org/10.1029/2023jc020494